ANALYSIS OF ROLL FORMING CONTINUOUS FIBRE-REINFORCED THERMOPLASTIC SHEETS

D. Bhattacharyya, R.J. Dykes, P.J. Hunter[†]
Centre for Composites Research, Private Bag 92019, University of Auckland, Auckland, New Zealand.
[†]*Department of Engineering Science, Private Bag 92019, University of Auckland, Auckland, New Zealand.*

SUMMARY

This paper details a roll forming study performed on sheets of continuous fibre-reinforced thermoplastic (CFRT) material. The deformation length, or transitional region over which the material deforms, is studied for various temperatures, laminate configurations, and roll settings using a surface grid strain technique. While the general shape adopted by the sheets is found to be largely independent of the laminate architecture and forming speed, the strain path would appear to be highly dependent on the way the individual layers of the sheet are orientated. The deformation is found to closely resemble that of a idealised trellis-type flow with negligible extension observed in the fibre directions. The geometric conformance of top-hat sections formed through the entire roll forming process is also analysed and compared to a simple numerical model. The kinematics of the process between two consecutive roll stations is also discussed.

INTRODUCTION

Fibre-reinforced thermoplastic composite materials have received considerable attention since their commercial inception in the early 1980s. This has been largely fuelled by the potential they have for rapid automated production, a key advantage that distinguishes them from their thermosetting composite counterparts. Thermoplastic matrices laced with large volumes of aligned continuous fibre-reinforcement may be formed into complex 3-dimensional components using heat and relatively low forces. This has led to the development of a variety of forming techniques which can generally be classified as thermo-forming processes. Other notable advantages that fibre-reinforced thermoplastic materials possess extend even further into the realms of performance, where they exhibit high specific strength and excellent toughness compared to other traditional materials such as steels and metal alloys. Despite these, and many other advantages, there remains a notable absence of economically efficient methods by which to process thermoplastic composite systems. Current sheet forming techniques tend to be costly and inefficient, with limited versatility. The need to develop faster more reliable processing methods, that make full use of the benefits of thermoplastic composites, is the key to their long term viability as structural and semi-structural materials.

One of the manufacturing technologies that appears likely to realise the full benefits of CFRTs is roll forming. Recently adapted from sheet metal forming, roll forming is a rapid processing operation used for transforming flat sheets of material into useful profiled sections. As shown in Figure 1, the method employs consecutive roll stations to progressively deform the strip into some desirable shape. The continuous nature of the process coupled with its versatility and speed make it an extremely attractive technique for producing light weight, structurally efficient components from sheet materials. Preliminary forming trials on CFRTs have been conducted by Cattanach *et al.* [1] but the degree of success and the methodologies employed remain unpublished. More recently Mander *et al.* [2] have published the results of a series of roll forming experiments conducted on Plytron®. The article describes the techniques used to increase the process reliability as well as formed part quality. The methods used to do this generally involved manipulating the temperature of the sheet in-situ.

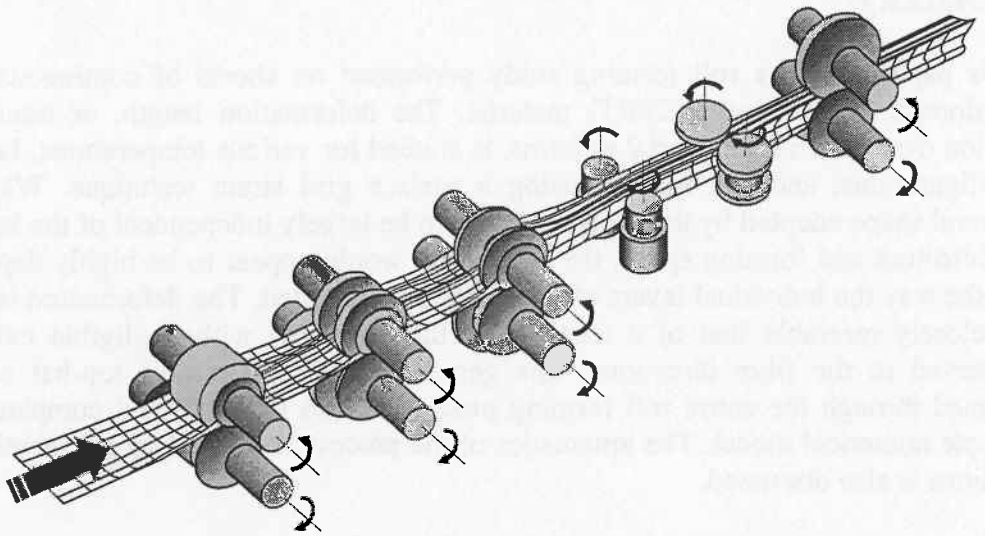

Figure 1. A schematic illustration of the roll forming process incorporating vertical as well as horizontal rolls.

Line speeds for a commercial roll forming operation range from 10-200m/min making it one of the most productive metal working processes in existence. Despite this, it was not until the demand for better and faster methods of producing sheet metal parts was recognised that its use became widespread [3]. Nowadays the process has found applications in many sectors including automotive, aerospace, construction, and transportation. As shown in Figure 2, the automotive industry in particular has made extensive use of roll forming to produce body moulding and trim, door headers, window guides, bumper reinforcements, seat tracks, and door impact bars. The potential of the process has even been recognised by the space industry who have identified it as a potential candidate for forming the building blocks of future space stations [4].

This paper focuses on two important aspects of the roll forming process: the deformation length and strain characteristics of sheets formed through the initial pass, and secondly, the geometric conformance of parts formed through the entire operation. In the first part of the paper, the implications of the deformation length are discussed and its relevance to the design of roll forming equipment is addressed. Though no comprehensive mathematical description of the process is offered, the kinematics of the forming operation is addressed. The next part of the paper outlines

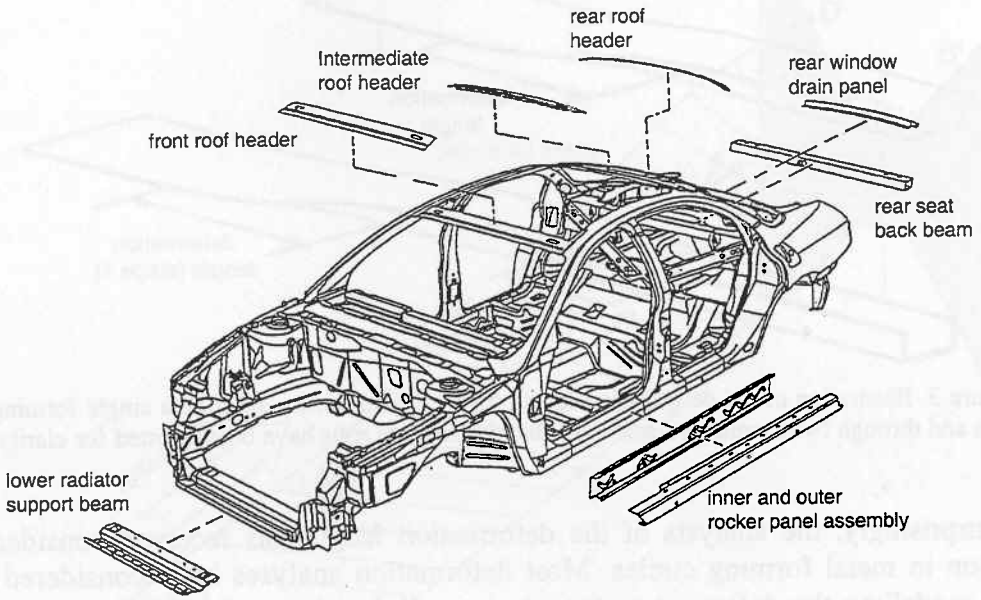

Figure 2. Roll formed components used in automobiles [5].

the experimental equipment and methods used to study the deformation length in a series of trials. The forming experiments are divided into two areas: The first experiments are set up to study the forming characteristics of various sheets through the initial forming pass. A surface grid strain analysis is undertaken, allowing the shape and forming path of the material to be established. The second set of experiments investigate the geometric conformance of roll formed top-hat sections. A simple finite element model is then introduced to predict the deformation observed in a series of top-hat sections. Finally, the main conclusions of this study are summarised.

The deformation length

Like most other sheet forming processes, roll forming can be considered a plane stress operation in which the sheet is made to bend and stretch over some region in order to conform to the shape of the rolls. Since the transition from a flat strip to the desired shape does not occur instantaneously the strip must gradually deform over some transitional length. This length has been coined as the *deformation length* within which the strip acquires a complex 3-dimensional geometry. Figure 3 illustrates the concept of the deformation length for a simple channel section formed through a single pass, and then through two passes. Within this region defects such as fibre wrinkling, edge buckling, and twisting of the section can occur. The occurrence of these defects can hinder the stability of the process and lead to unacceptable product irregularities. The deformation region is therefore an important facet of the process that must be understood if the technique of roll forming is to be successfully applied to reinforced thermoplastic sheets.

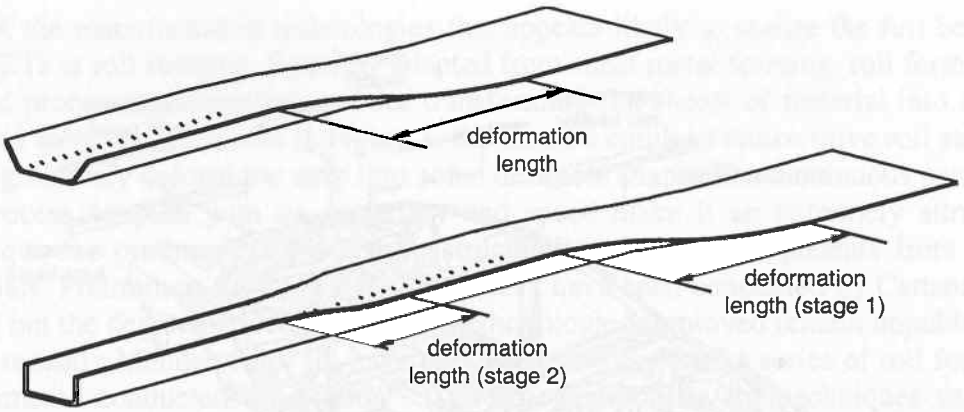

Figure 3. Illustration of the deformation length for a channel section through a single forming pass and through two forming stages. Note that the forming rolls have been omitted for clarity. [6].

Not surprisingly, the analysis of the deformation length has received considerable attention in metal forming circles. Most deformation analyses have considered two areas: modelling the deformed surface during roll forming and modelling the strain distribution in the sheet during forming. By minimising the work done due to transverse bending and stretching, Bhattacharyya *et al.* [7] were able to derive a useful expression for the deformation length of a simple channel section. Interestingly, the expression obtained consisted entirely of geometric variables even though a rigid-perfectly plastic material model was assumed in the analysis. Experimental evidence generally supports the relationship for a variety of metallic materials despite the fact that the model neglects the effects of the rolls. Since thermoplastic composite materials behave like viscous fluids during forming, there is no reason why a similar approach can not be employed to predict the deformation in a CFRT sheet. By assuming that the sheet adopts a configuration that minimises the rate of energy being dissipated by the fluid a suitable solution should be achieved.

Given the geometric complexity of the operation and the non-unique boundary conditions it is difficult to conceive that a closed form solution could be obtained through analytical means. On the other hand, numerical methods are well suited to this type of problem. The following section details how the kinematics of the problem can be formulated using a Lagrangian approach. Specifically, we demonstrate how the strain rate tensor can be written independently of time for a steady state deformation.

Kinematic approach to roll forming

The key to analysing strain in a material undergoing large deformations is to establish two types of coordinate systems and develop a relationship between them. The first are fixed reference or spatial coordinates (x,y,z) and the second (material coordinates) are embedded in the deforming body (v_1,v_2,v_3). The kinematics of the deforming body can then be defined by the relationship between the reference x_i - coordinates and the material v_M - coordinates in the deformation gradient tensor which is written as

$$F_M^i = \frac{\partial x_i}{\partial v_M} \tag{1}$$

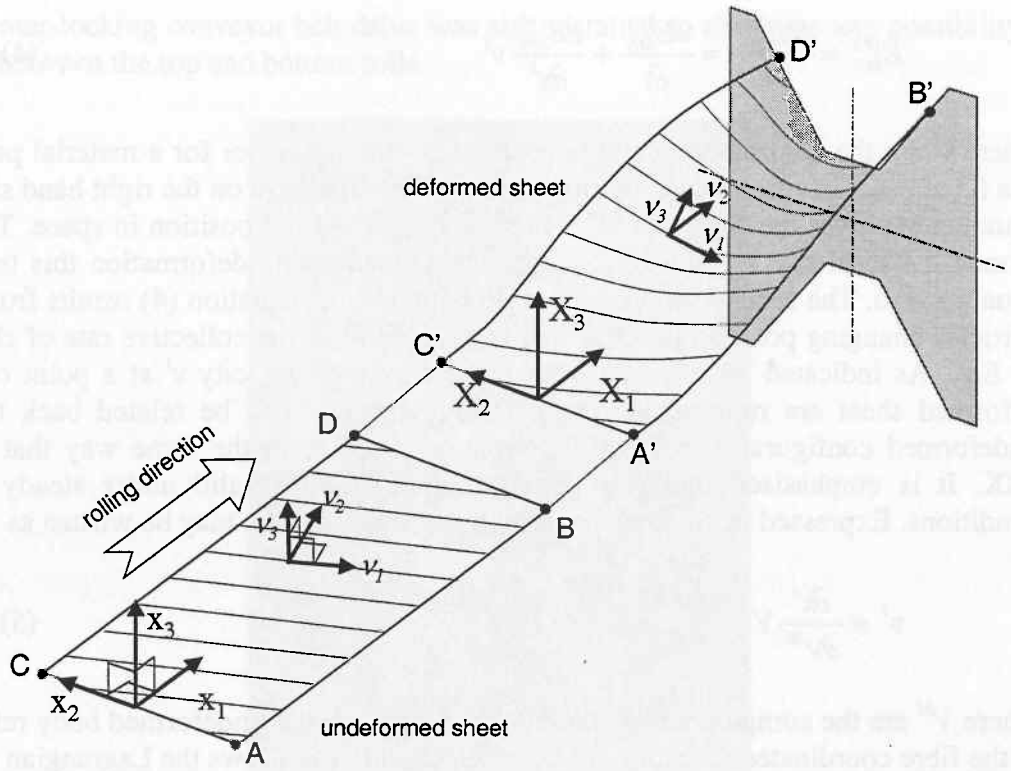

Figure 4. The undeformed and deformed sheet with spatial (x_1,x_2,x_3) and material (v_1, v_2, v_3) coordinate systems. Note that the shaded region represents the cross-section of the circular female forming roll.

As shown in Figure 4, we chose the v_M – coordinate directions to coincide with certain features of the undeformed fibre reinforced sheet: v_1 is aligned with the fibre directions, v_2 is aligned in the plane of the sheet, and v_3 is normal to the sheet surface. In the undeformed sheet the v_M – coordinates form an orthogonal coordinate system. From the deformation gradient, the following Lagrangian quantities can be established

$$C_{MN}^{(v)} = \frac{\partial x_i}{\partial v_M}\frac{\partial x_i}{\partial v_N} = \mathbf{F}^{\mathrm{T}}\mathbf{F} \tag{2}$$

$$E_{MN}^{(v)} = \tfrac{1}{2}\left(C_{MN}^{(v)} - \delta_{MN}\right) \tag{3}$$

C_{MN} is termed the Green deformation tensor or right Cauchy-Green tensor. **C** possesses material coordinate (upper case) indices indicating that this tensor is only dependent on material coordinates and is therefore independent of any rigid body motions. E_{MN} is the Lagrangian strain tensor the components of which are zero when the material is undeformed. For small strain, **E** becomes the strain tensor of classical linearized elasticity theory. Similar Eulerian strain and deformation tensors can just as easily be developed in terms of the spatial x_i – coordinates using the inverse of the deformation gradient tensor.

The Lagrangian strain rate tensor can be evaluated as the material, or total time derivative of **E** (in a spatial sense). Thus

$$\dot{E}_{MN}^{(v)} = \frac{DE_{MN}^{(v)}}{Dt} = \frac{\partial E_{MN}^{(v)}}{\partial t} + \frac{\partial E_{MN}^{(v)}}{\partial x^i} v^i \tag{4}$$

where v^i are the contravariant components of a velocity vector for a material particle at a fixed point in space on the deformed body. The first term on the right hand side of equation (4) gives the time rate of change of E_{MN} at a fixed position in space. This is termed the local rate of change E_{MN} and for a steady state deformation this term is equal to zero. The second term on the right hand side of equation (4) results from the particles changing position in space and is referred to as the collective rate of change of E_{MN}. As indicated by the index, the components of velocity v^i at a point on the deformed sheet are referred to spatial coordinates but can be related back to the undeformed configuration via the deformation gradient in the same way that $\mathbf{dx} = \mathbf{F}d\mathbf{X}$. It is emphasised that this transformation is only valid under steady state conditions. Expressed in component form, this transformation may be written as

$$v^i = \frac{\partial x^i}{\partial v^M} V^M \tag{5}$$

where V^M are the components of velocity for a point on the undeformed body referred to the fibre coordinates. Substituting equation (5) into (4) allows the Lagrangian strain rate tensor to be written as

$$\dot{E}_{MN}^{(v)} = \tfrac{1}{2}\dot{C}_{MN}^{(v)} = \frac{V_0}{2}\left(\frac{\partial C_{MN}^{(v)}}{\partial v^1}\cos\phi + \frac{\partial C_{MN}^{(v)}}{\partial v^2}\sin\phi \right) \tag{6}$$

where V_0 is the linear velocity of the sheet and ϕ is the angle between the fibres and the rolling direction. Note that equation (6) assumes that the undeformed sheet has no velocity in the x_3 direction. Nefussi and Gilormini used a similar kinematic model for predicting the deformed shape and deformation length in a metallic cold roll forming operation [8]. Their choice of shape functions however placed theoretical restrictions on the predicted surface. With the addition of certain kinematic constraints, the tensor may be utilised within the framework of the ideal fibre reinforced material model. A suitable finite element scheme could then be employed to solve for the deformed configuration subject to the appropriate boundary conditions. The most significant advantage of this approach, is that the problem can attacked using the same methodologies used for dealing with finite elasticity problems. The entire theory pertaining to the computational analysis of the deformation length has been derived and will be formally outlined in a future article by the authors. For the time being though, we concentrate on the practical aspects of the forming process.

EXPERIMENTAL DETAILS

An experimental study of the roll forming process was undertaken using a modified horizontal beam raft-type roll forming machine. The machine, shown in Figure 5, had five individual forming stations at 275 mm spacing, and was powered by a 4.4kW induction motor fitted with an infinitely variable speed controller. The gear reduction allowed linear line speeds of between 0.1-10m/min. The bottom roll shafts of the roll former were interconnected and driven by a 21 tooth sprocket and chain arrangement.

An inter-locking conveyor belt drive was also installed to eliminate any possibility of slip between the top and bottom rolls.

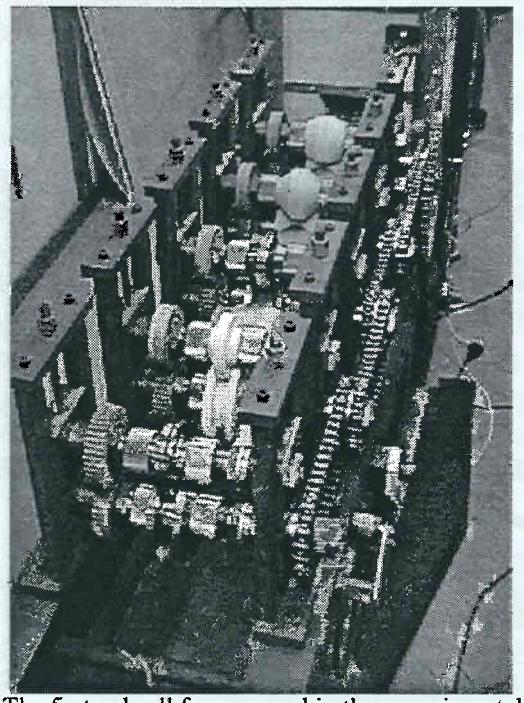

Figure 5. The 5-stand roll former used in the experimental analysis.

A summary of the specifications for the roll forming machine are provided in Table 1. A notable feature of the roll former is the limited number of modifications which have been made from the "as delivered" configuration. Apart from the preheating oven and various other minor ancillary devices, the machine, in the described configuration, remained capable of forming sections from medium gauge aluminium sheet.

Table 1. Roll former specifications.

Type:	Horizontal Beam Raft (light-medium gauge)
Number of stands:	5
Shaft diameter:	40 mm
Stand width:	350 mm
Drive:	Bottom – Chain via 3 phase AC 410 volt Top – conveyor belt friction drive via bottom roll
Speed control:	Infinitely variable speed, 0.1 - 10.0 m/min
Roll stand pitch:	275 mm
Vertical Adjustment:	Manual screw thread - 75 mm
Roll Material:	1040 Steel, Delrin™ plastic

A preheating oven and feeding system capable of supplying long semi-continuous lengths of pre-consolidated thermoplastic composite sheet was designed and constructed specifically for this investigation. The oven, shown in Figure 6, consisted of a series of halogen elements arranged along its length. The 9 elements, capable of delivering a total of 6.4kW, were mounted above a 115mm wide stainless steel conveyor belt. The halogen elements were attached to the underside of a reflective stainless steel sheet which formed the roof of the oven. The proximity of the elements to the strip could be varied by utilising the adjustable supports which were attached to the upper side of the oven roof. The transportation of the strip through the oven and into the forming operation was facilitated by means of a conveyor belt arrangement

which was connected to, and driven via the main drive motor. After a series of preliminary trials it was found that the stainless steel belt required an additional insulating medium to prevent the conduction of heat from the strip to the belt. For this purpose, narrow strips of Teflon sheet measuring 2 mm in thickness were cut and fixed to the belt.

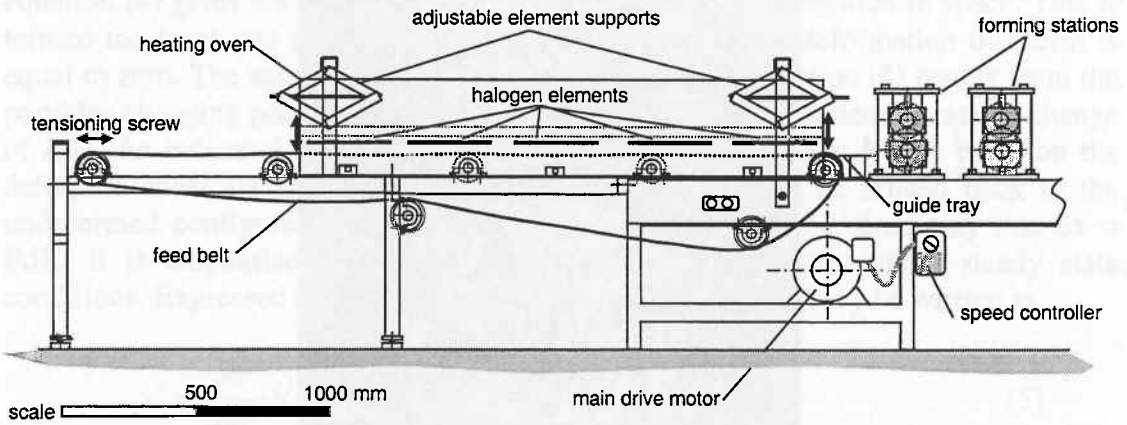

Figure 6. A side view of the heating and transportation device used for supplying semi-continuous strips to the roll former.

The roll forming experiments were conducted using Plytron sheets (a polypropylene/glass fibre unidirectional pre-impregnated material with a nominal fibre volume fraction of 35%). The overall dimensions of the samples tested are detailed in Figure 7. All samples were consolidated from 8 plies of prepreg, each ply having a nominal thickness of 0.25mm. Consolidation was performed at a temperature of 200°C under a vacuum pressure of 6kPa. The control axis (or 0° axis) was defined in the longitudinal direction of the strips. Each sample was consolidated with a K-type thermocouple embedded in the centre of the laminate as shown in Figure 7.

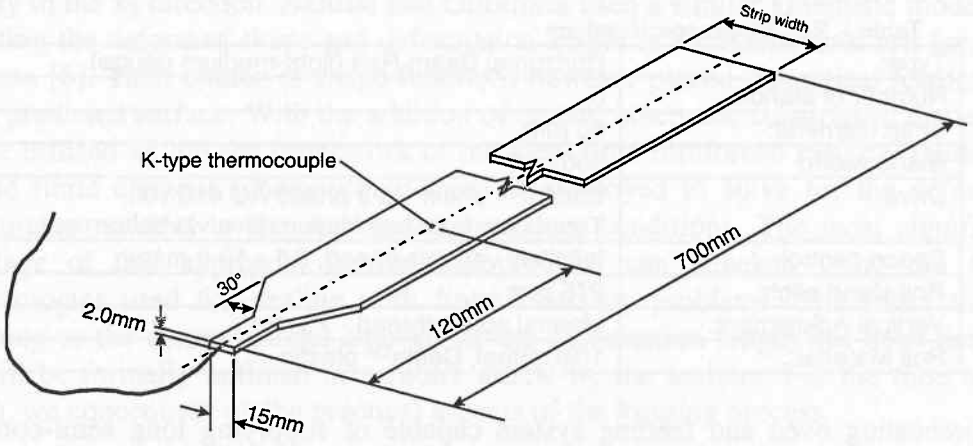

Figure 7. Dimensions of consolidated strips used in roll forming experiments.

The other variables investigated in the deformation trials were the forming increment (or roll angle), forming speed, and flange length. These processing parameters were investigated using an inlet temperature of 140°C with $[0°/90°/90°/0°]_S$ laminates exclusively. Flange lengths of 20, 25, 30, 35, and 40 mm were investigated using a 30° roll angle at a line speed of 5 m/min. The flange lengths of samples used in all the other trials was kept constant at 35 mm. The surface strain characteristics were examined using a 5 mm square grid pattern screen printed on the upper surface of

each sample. Each grid pattern was subsequently digitised using a 3-dimensional digitising package developed at the University of Auckland. This data was then analysed using a grid strain analysis (GSA) package the details of which have been outlined in an article by Martin *et al.* [10].

The procedures used to form each sample were as follows: samples were positioned on the feed belt just prior to the inlet of the heating oven. The thermocouple wire was fed through the oven and forming rolls which allowed it to be pulled through at the same rate at which the strip was being formed. The temperature measured by each thermocouple wire was monitored through the entire heating and forming process. Suitable heating procedures were established over a variety of forming speeds during the commissioning of the oven. In each case the temperature of the strip was raised to 190°C prior to forming. After this initial heating stage, the belt was stopped and the strip allowed to cool before commencement of forming. Samples rolled through the entire process were formed using the flower diagram detailed in Figure 8. The dimensions of the intended top-hat section are shown in Figure 9.

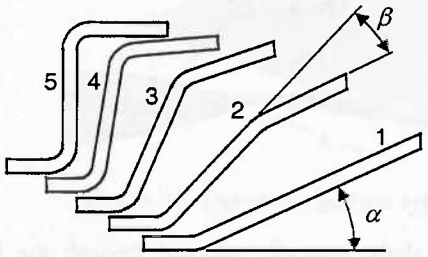

	Roll angles	
Roll station #	α°	β°
1	30	0
2	47	21
3	67	48
4	81	76
5	90	90

Figure 8. Flower pattern used in roll forming trials

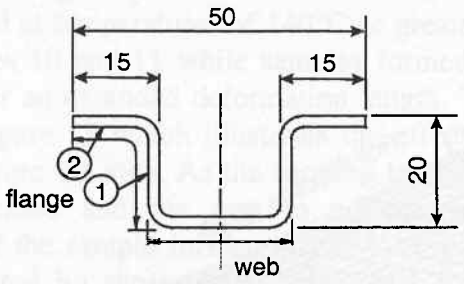

Figure 9. Dimensions of top-hat section.

For the initial forming trials performed through the first set of rolls a quenching agent was used to freeze or fix the sheet in its steady state configuration. As the roll forming operation was stopped, chilled water was sprayed over the deformed sheet through a perforated copper coil. This was done to prevent the sheet from wilting under its own weight thus ensuring a reasonably accurate representation of the steady state configuration.

RESULTS AND DISCUSSION

Figures 10 and 11 show an example of the 3-dimensional shape typically adopted by the samples formed through the initial pass at temperatures of 140°C or greater. It is to be noted that polypropylene composites, such as Plytron, exhibit an extended

processing window from the melt which enables them to be formed at temperatures as low as 100°C. Therefore, when processing temperatures are stated it is implied that the sample has been heated to 180°C and then cooled to the quoted value. Each mesh was generated from digitised data that was processed through the GSA program. The deformed surface in both Figures has been divided into three zones: region A, where the strip remains unaffected by the rolls or deformation downstream, region B, where the sheet experiences deformation but is not in contact with the forming rolls, and region C, where the sheet deforms while in contact with the rolls.

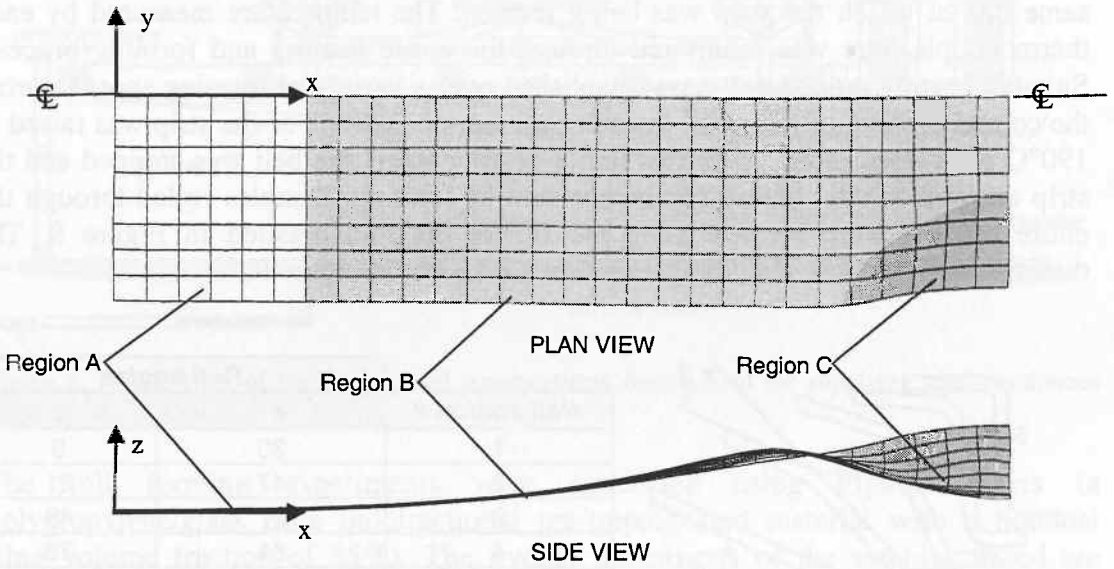

Figure 10. A digitised surface showing the characteristic shape typically adopted through the first forming pass. Note that only half the section is shown due to symmetry. ($[0°/90°/90°/0°]_S$, forming speed = 5 m/min, inlet temperature = 140°C, flange length = 35 mm)

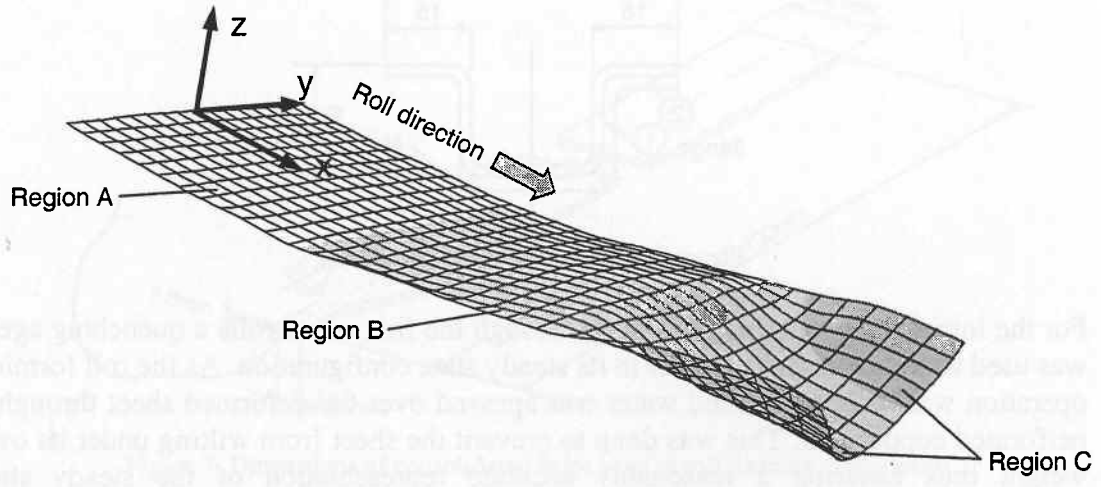

Figure 11. A typical surface representation of a partially deformed sheet formed through the first pass.

Virtually all the deformation appears to take place in the transition between regions B and C, where the sheet comes into contact with the forming rolls. While region B generally encompasses a much lager portion of the sheet than region C, only a minimal amount of bending, mostly in the longitudinal direction, would appear to take place there. As illustrated by the side view in Figure 10, almost all the transverse

bending required to form the flange takes place as the sheet comes into contact with the rolls. This is in contrast to sheet metals which tend to bend and stretch over the entire transition region prior to contacting the rolls [7]. Zhu *et. al* [9] have presented experimental evidence to suggest the flange length remains constant and develops about a definite plastic hinge through the transition region. Accordingly the deformed flange in sheet metal can be described by some function $\theta(x)$ as shown in Figure 12. However, it is unlikely that a similar geometric model could be used to describe the deformed surface in CFRT sheets as the flange length appears to vary with x and y.

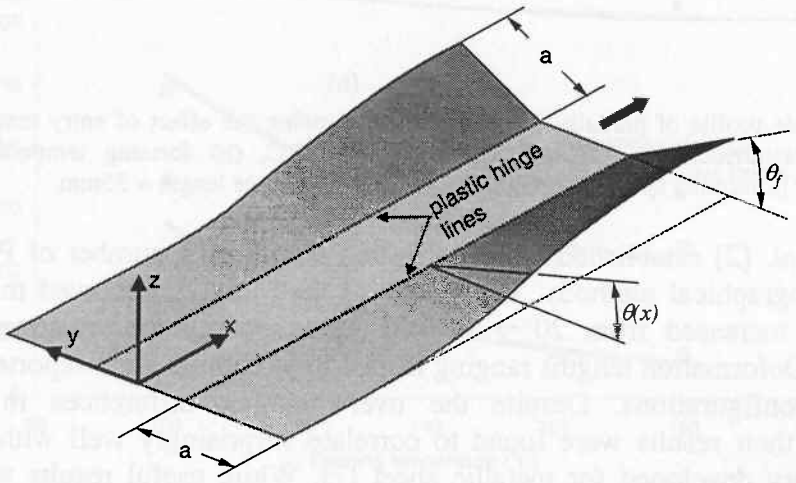

Figure 12. Deformed surface typically encountered in roll forming of metallic sheet.

The characteristic shape adopted by the sheet (Figures 10 and 11) remained largely unaffected by any variation in fibre architecture, forming speed, and flange length. Predictably though, the forming temperature was found to have a significant effect on the shape. Samples formed at temperatures of 140°C or greater generally adopted the shape illustrated in Figures 10 and 11 while samples formed at temperatures below 140°C tended deform over an extended deformation length. The difference in shape can be clearly seen in Figure 13 which illustrates the effect of temperature on the forming process viewed from the side. As the forming temperature was lowered, the deformation length increased and the area in contact with the rolls reduced. Interestingly, the shape of the sample formed at 120°C (Figure 13(b)) bears a close resemblance to that adopted by sheet metals where the flange develops over the majority of the deformation length. This result clearly demonstrates how the behaviour of the material becomes increasingly elastic, and less viscous, as the forming temperature approaches the lower limits of the temperature forming window. Since entry temperatures lower than 140°C were found to result in forming problems downstream, this behaviour would seem less relevant to the initial part of the process than to the final stages of the process.

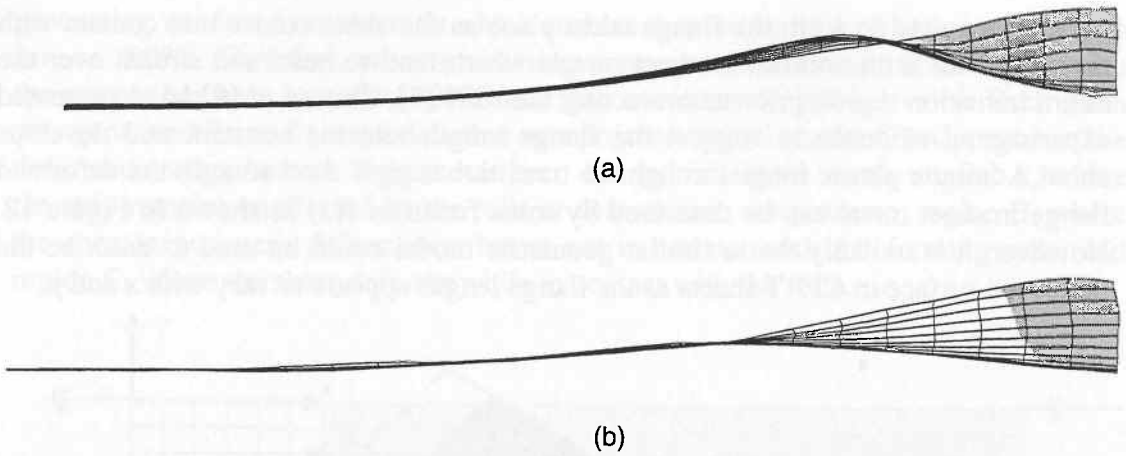

Figure 13. Side profile of partially deformed sheets showing the effect of entry temperature on the forming characteristics (a) forming temperature = 140°C, (b) forming temperature = 120°C. $[0°/90°/90°/0°]_S$, forming speed = 5m/min, roll angle = 30°, flange length = 35mm.

Mander *et al.* [2] established the deformation length of a number of Plytron sheets using photographical methods. The results of their analysis showed that as the roll angle was increased from 20°→30°→40°, the apparent deformation length also increased. Deformation lengths ranging from 150 to 250mm were reported for various laminate configurations. Despite the overwhelming differences in constitutive behaviour, their results were found to correlate surprisingly well with deformation length theory developed for metallic sheet [7]. While useful results were obtained from their trials no details pertaining to the forming characteristics were presented or discussed by the authors. From the results presented in the previous section it is clear that the deformation length can be measured using two different approaches: the primary deformation length (L_1), which is measured upstream from the roll centre to the initiation of transverse bending, and the secondary deformation length (L_2), which encompasses L_1 as well as the portion of the strip that deforms by bending in the longitudinal direction. These lengths are defined in Figure 14 and were measured for each successfully formed sample.

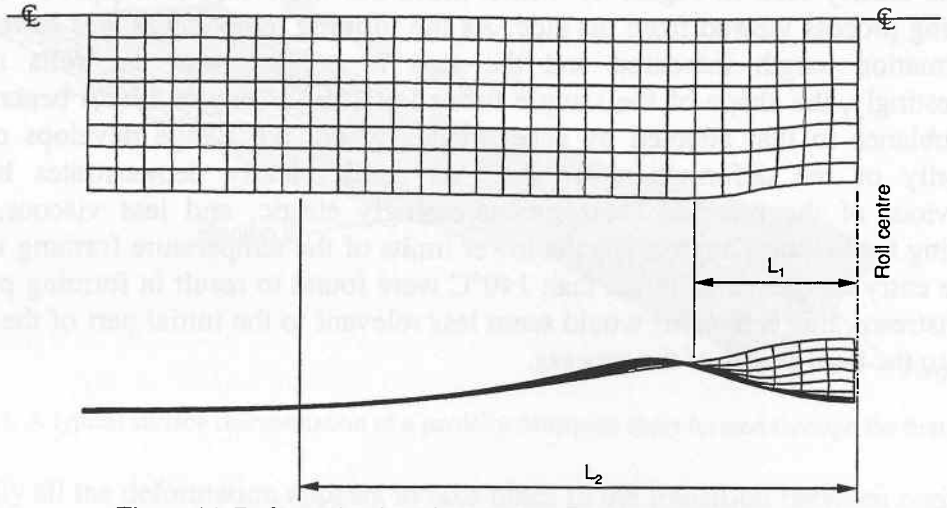

Figure 14. Deformation lengths, primary (L_1) and secondary (L_2).

The deformation lengths of a number of $[0°/90°/90°/0°]_S$ samples formed over a variety of temperatures have been plotted in Figure 15. The results show that as the temperature is increased, both the primary and secondary deformation lengths

asymptote to a minimum value. As was shown in the previous section, the primary deformation length for sheets formed at temperatures of 140°C or greater, could be predicted by considering the geometry of the roll. This is because the flange does not begin to develop until the sheet comes in contact with the forming rolls. As the temperature is decreased, the deformation lengths increase as the elastic response of the material becomes more pronounced. Despite the differences in experimental methods, the deformation length measurements reported by Mander *et al.* would appear to correlate reasonably with the secondary deformation lengths measured in this study.

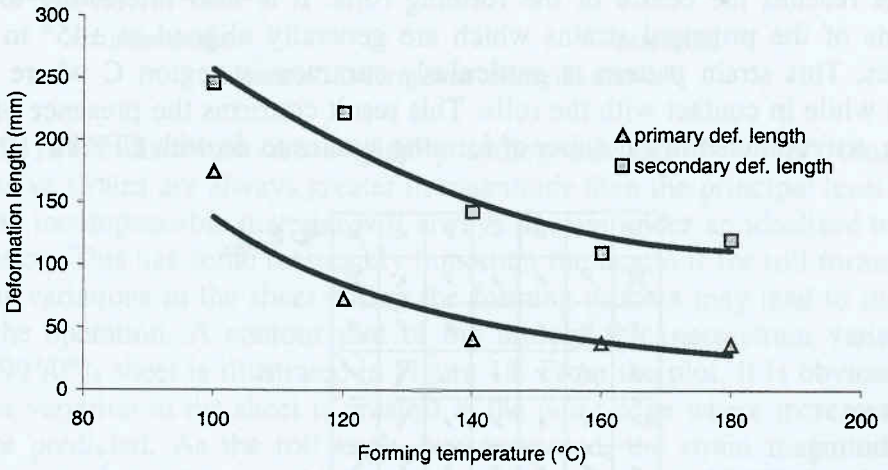

Figure 15. Deformation lengths of $[0°/90°/90°/0°]_S$ sheets formed through 30° rolls at various temperatures. Forming speed = 5m/min, flange length = 35mm.

The next part of the paper details the results from the large strain analysis performed on a series of samples which were fed through the first forming increment. The grid strain results presented herein are illustrated in two different ways: strain arrow diagrams, which indicate the magnitudes and directions of principal surface strains within each deformed grid, and thickness strain plots, which provide a means of assessing the thickness variation through the sheet. Since GSA uses data from both the initial and final configurations, the results may be presented in terms of the undeformed or deformed states. While a number of authors have applied the technique to various types of thermoplastic composite systems in the past, none have used it to investigate the distribution of strain through a continuous process like roll forming. The novel way in which it is applied here means that a unique strain path can be determined directly from the deformed surface which is unlike typical grid strain analyses which consider just the initial and final states only.

The systematic error, incurred when digitising each deformed sheet, was found to be approximately 0.01 mm. With the original grid spacing equal to 5.0 mm, this error could have resulted in strain errors of up to 2%. A note of caution should therefore be issued regarding areas of relatively small strain. The principal axes in such areas could be substantially affected by the slightest of errors incurred during the digitising process. Consequently, the trends exhibited in the results should be noted rather than the absolute strain magnitudes and directions in each element. Other practical difficulties were also encountered at forming temperatures greater than 180°C. At these higher temperatures, the surface layer tended to become smudged so that no meaningful data could be extracted.

Figure 16 shows the strain distribution on the undeformed surface of a $[0°/90°/90°/0°]_S$ laminate, which was formed through an initial roll angle of 30° at a temperature of 140°C. The undeformed surface fibres, which are aligned with the rolling direction, are illustrated by a series of solid lines, while the fibres of the sub-surface layers are illustrated by a series of dotted lines. As anticipated, the strain magnitudes are greatest at the roll end of the sheet (Region C), where the sheet adopts the shape of the forming rolls. In fact the position of greatest principal strain, denoted by ε_{max} in the diagram, is located on the outer portion of the flange just prior to where the sheet reaches the centre of the forming rolls. It is also interesting to note the directions of the principal strains which are generally aligned at ±45° to the fibre directions. This strain pattern is particularly common in region C where the sheet deforms while in contact with the rolls. This result confirms the presence of in-plane shearing, a trend noted in a number of forming studies to do with CFRTs [10, 11].

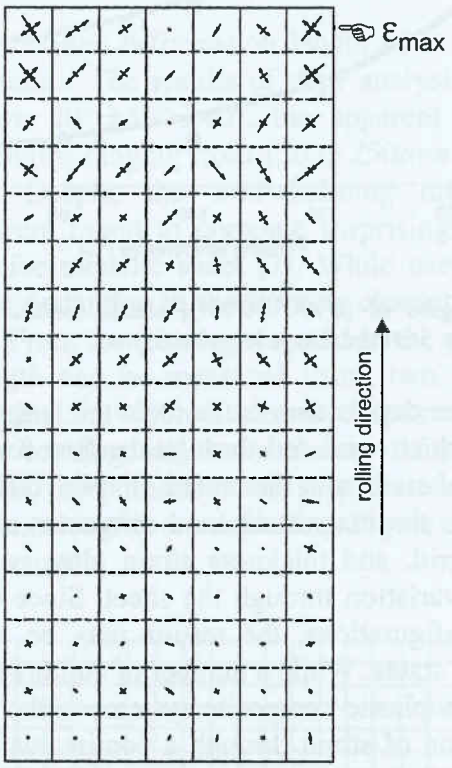

Figure 16. Principal strain arrow plot shown over the undeformed surface for $[0°/90°/90°/0°]_S$ sample. Forming temperature =140°C, roll angle = 30°, flange length = 35mm. ε_{max} = 10.9%, ε_{min} = -11.1%.

As observed by Martin *et al.* [10] the fibre lengths appear to remain unchanged as the flange of the sheet develops by in-plane shearing. This mode of deformation has been described as a trellis action by Cattanach *et al.* [12], as the extension of a trellis in one direction is accompanied by a contraction in the other direction. The kinematics of these inextensible fibre networks, often referred to as Chebyshev nets, has been addressed by a number of authors [13, 14]. Using the geometry in Figure 17, the true principal strains, ε_1 and ε_2, can be established in terms of the extension ratios, λ_1 and λ_2 by

$$\varepsilon_1 = \ln(\lambda_1) = \ln\left(\frac{\cos\theta}{\cos\Phi}\right) \qquad \varepsilon_2 = \ln(\lambda_2) = \ln\left(\frac{\sin\theta}{\sin\Phi}\right) \qquad (1)$$

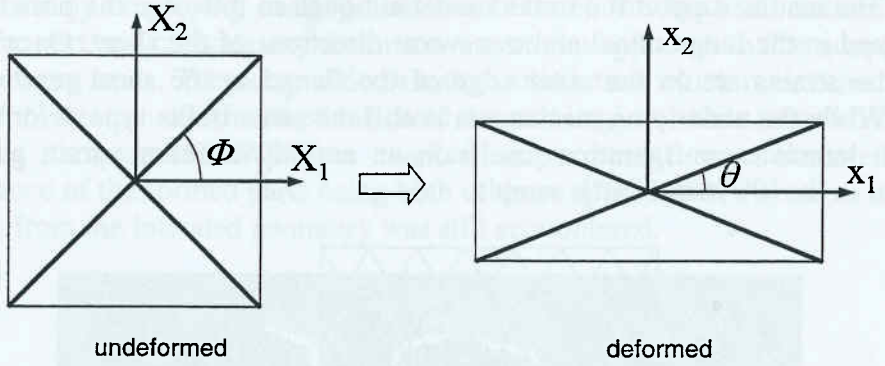

Figure 17. Deformation of a trellis network.

When the fibre directions are originally orthogonal, i.e. Φ = 45°, the principal compressive strains are always greater in magnitude than the principal tensile strains, so that an incompressible material will always thicken under an idealised trellis type deformation. This has some reasonably important implications for roll forming where thickness variations in the sheet during the forming process may lead to instabilities within the operation. A contour plot of the through-thickness strain variation in a $[0°/90°/90°/0°]_S$ sheet is illustrated in Figure 18. From the plot, it is obvious that the thickness variation in the sheet is greatest at the outer edge where increases of up to 7.3% are predicted. As the roll angle was increased, the strain magnitudes in the flange increased, resulting in thickness increases as high as 13.2% for the 40° roll setting. Since the roll angle influences the magnitude of the shear deformation in the flange of the sheet, this effect obviously needs to be carefully considered in the design of the forming rolls and roll gap settings.

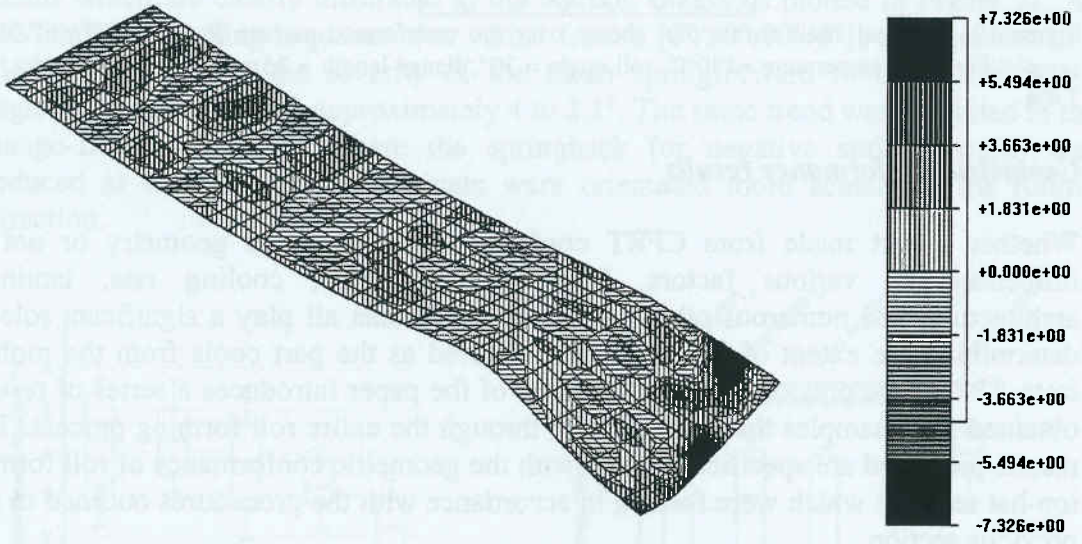

Figure 18. Contour plot of through thickness strain in the deforming sheet (note that only half the sheet is shown due to symmetry). Laminate architecture = $[0°/90°/90°/0°]_S$, Forming temperature =140°C, roll angle = 30°, flange length = 35mm.

The same concept may be further investigated by considering the deformation of a bi-directional laminate where the fibre orientations are skewed from the rolling direction. Figure 19 shows the principal strain distribution on the undeformed surface of a [30°/-

$30°/-30°/30°]_S$ laminate formed through an initial roll angle of 30° at a temperature of 140°C. The results support the trellis model although in this case the principal strains are aligned in the longitudinal and transverse directions of the sheet. Once again, the maximum strains act on the outer edge of the flange as the sheet reaches the roll centre. While the underlying mechanism is still the same trellis type deformation, the different laminate configuration results in an entirely different strain path to that observed in the $[0°/90°/90°/0°]_S$ sample.

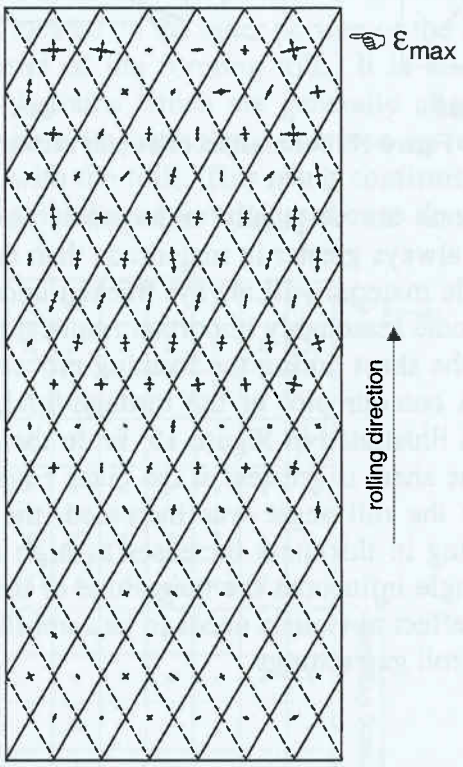

Figure 19. Principal strain arrow plot shown over the undeformed surface for $[30°/-30°/-30°/30°]_S$ sample. Forming temperature =140°C, roll angle = 30°, flange length = 35mm. ε_{max} = 12.3%, ε_{min} = -7.4%.

Geometric conformance results

Whether a part made from CFRT conforms to its intended geometry or not is influenced by various factors. Forming temperature, cooling rate, laminate architecture, and numerous other process variables can all play a significant role in determining the extent of any distortion incurred as the part cools from the molten state. Unlike the previous section, this part of the paper introduces a series of results obtained from samples that were formed through the entire roll forming process. The results presented are specifically to do with the geometric conformance of roll formed top-hat sections which were formed in accordance with the procedures outlined in the previous section.

Generally, the geometric conformance of the parts that were formed through the entire roll forming process was poor, with deviation around bend regions of up to 12.5° from that of their intended formed part angle. A number of cut-away sections, revealing the typical levels of distortion around the bend regions, are shown in Figure 20. Surprisingly, the sections were found to exhibit springforward around the web/flange-1 region as well as springback in the flange-1/flange-2 region. Mander *et al.* [2] also

encountered the same effect in their studies, but showed how the conformance could be improved by employing cooling elements between the final roll stations so as to quench the part and mitigate any distortion – a similar approach to that adopted in the partial forming trials. They also added another roll station which maintained the final profile of the section which effectively held the part in place while it cooled below the solidifying temperature. While a marked improvement was observed in the conformance of the formed parts using both of these approaches, a nominal amount of deviation from the intended geometry was still encountered.

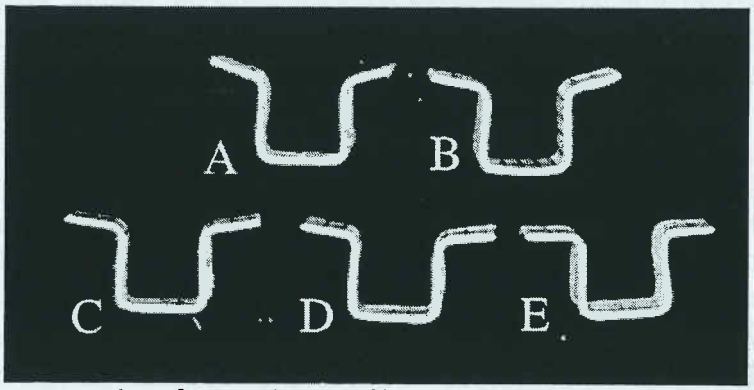

Figure 20. Cut-away sections from various profiles. (A) $[0°/90°/90°/0°]_S$, (B) $[90°/0°/0°/90°]_S$, (C) $[45°/-45°/-45°/45°]_S$, (D) $[30°/-30°/-30°/30°]_S$, (E) $[15°/-15°/-15°/15°]_S$. Note the locality of the springforward in the web/flange-1 region and springback in the flange-1/flange-2 region.

The analysis of the profiles that were formed through the entire process involved measuring the formed part angles in the flange-1/flange-2 region and the web/flange-1 region. Four measurements were made at increments of 50 mm along the length of each specimen. For each laminate type a total of 15 measurements were made for each active bend region. The statistical analysis of the deviation revealed some interesting trends which are clearly illustrated in the whisker diagrams plotted in Figure 21. As the laminate stacking sequence was varied from a $[0°/90°/90°/0°]_S$ arrangement to a $[15°/-15°/-15°/15°]_S$, the severity of the mean springforward in the web/flange-1 region was reduced from approximately 4 to 2.1°. The same trend was exhibited in the flange-1/flange-2 region where the springback (or negative springforward) was reduced as the plies of the laminate were orientated more acutely to the rolling direction.

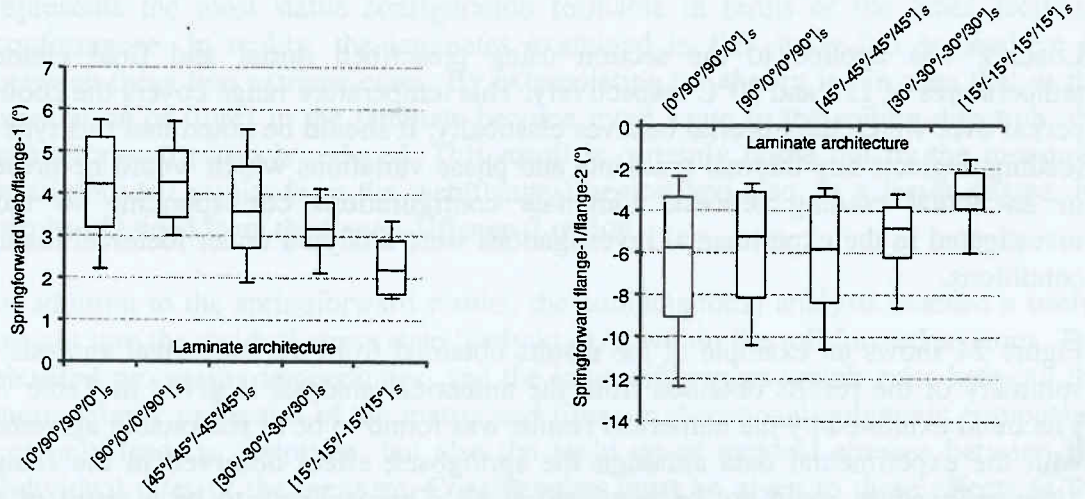

Figure 21. Statistical whisker plot of springforward results from web/flange-1 and flange-1/flange-2 bend regions. Forming speed = 5m/min, inlet temperature 140°C, flange length = 35mm.

The springforward effect observed in the roll formed sections has been studied by a number of authors who have generally simulated the effect using thermoelastic models [15, 16, 17]. Such an approach is relatively straight forward to apply, and can be readily formulated using standard computational methods. For instance, Zahlan and O'Neil [18] used a simple numerical model to predict the springforward effect in a number of 2- and 3-dimensional top-hat sections constructed from carbon fibre/PEEK (APC-2). Their analysis, based on a thermoelastic finite element model, yielded good correlation with their experimentally achieved results. With their success in mind, a similar type of analysis was undertaken to predict the deviation observed in samples formed in this study.

The Lusas® finite element system was used to create and analyse the computational model shown in Figure 22. The model itself was constructed in a 2-dimensional Cartesian reference frame using 2-d isoparametric plane strain elements. The cross sectional shape of the model was derived from the dimensions detailed in the last section although only half of the section was analysed due to symmetry. In keeping with the model of Zahlan and O'Neill, the material was treated as a transversely isotropic elastic solid over the entire cooling temperature range. The thermo-mechanical properties used in the analysis were obtained from [19].

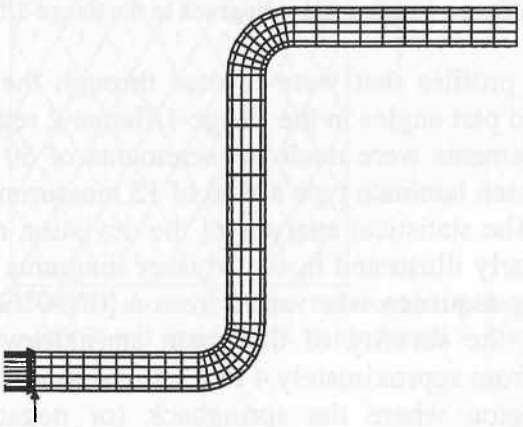

Figure 22. Computational model used in the springforward analysis (note that only half the model is shown due to symmetry).

Loading was applied to the section using prescribed initial and final element temperatures of 120 and 20°C respectively. This temperature range covers the cooling period over which the material behaves elastically. It should be noted that this type of loading neglects any thermal gradients and phase variations which would be present in an actual cooling process. Laminate configurations corresponding to those investigated in the experimental investigations were analysed under identical loading conditions.

Figure 24 shows an example of the results obtained from the numerical analysis. A summary of the results obtained from the numerical analysis is given in Table 7.1. The trend exhibited by the numerical results was found to be in reasonable agreement with the experimental data although the springback effect observed in the flange-1/flange-2 region could not be predicted at all. This is likely to be a result of the temperature gradients around the edge of the strip that have not been considered as

part of this analysis. In reality the strip loses heat as it contacts the forming rolls. By considering Figures 10 and 11 it is apparent that the outer portion of the strip is in contact with the rolls for a longer period of time than the centre portion of the strip.

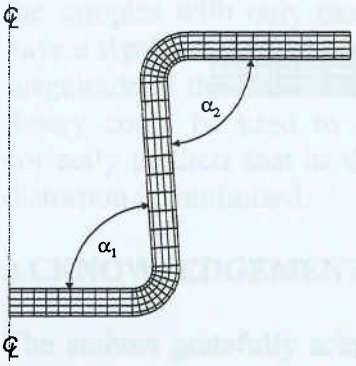

Figure 24. Deformed mesh after cooling

Table 7.AA. Comparison of springforward results, measured and predicted.

Laminate configuration	measured avg.		predicted	
	θ_1	θ_2	θ_1	θ_2
$[90°]_8$	-	-	86.42°	86.42°
$[0°/90°/90°/0°]_S$	85.67°	95.82°	87.03°	87.03°
$[90°/0°/0°/90°]_S$	85.63°	95.20°	87.53°	87.53°
$[45/-45/-45/45]_S$	86.39°	95.95°	88.82°	88.82°
$[30°/-30°/-30°/30°]_S$	86.81°	94.82	88.98°	88.98°
$[15°/-15°/-15°/15°]_S$	87.82°	93.22°	89.21°	89.21°
$[0°]_8$	-	-	90°	90°

While the magnitude of the springforward in the web/flange-1 region can not be accurately predicted using a thermoelastic model, the basic theory behind the approach does however lend itself towards explaining the trend observed in the results. The theoretical springforward angle in an orthotropic section may be described by

$$\Delta\theta = \theta(\alpha_T - \alpha_\theta)\Delta T \qquad (2)$$

where θ is the intended formed part angle, ΔT is the temperature range over which the part cools, and α_T and α_θ are the respective through-thickness and circumfrential thermal expansion coefficients. For roll formed Plytron sections, the maximum springforward can be anticipated when all the fibres are aligned at 90° to the rolling axis. In this hypothetical scenario, which is included in the results table above, the difference between the two thermal expansion coefficients is a maximum. However, when the fibres are stacked in the rolling direction, the cross section reassembles that of a homogenous material with the difference in thermal expansion coefficients being equal to zero. This laminate type, which is also included in the results table, obviously represents the most stable configuration formable in terms of the cross sectional conformance. In reality, the laminates examined in this study fell somewhere in between these two extreme cases. By extrapolating the theory it can seen that as the orientation of fibres in the laminate become more acute to the rolling direction, the springforward effect is reduced. This result is certainly borne out by the measured springforward results from the web/flange-1 region and also, to a lesser degree, by results obtained from the flange-1/flange-2 region.

In addition to the springforward results, the computational analysis enabled a useful insight into the residual stress state likely to exist within the roll formed sections. The elevated processing temperatures, and the large differences which exist between the thermoelastic properties of the matrix and fibres in directional polymeric composites not only leads to distortion, but also the build up of residual stresses between the individual plies of the laminate. Consideration must be given to these effects as the stresses can severely limit both the static and dynamic strength of the part. The

contours of stress in a $[0°/90°/90°/0°]_S$ section have been plotted in Figure 25. The stresses, given in kPa, are relatively low considering the laminate is constructed from layers which are orientated at 90° to one another.

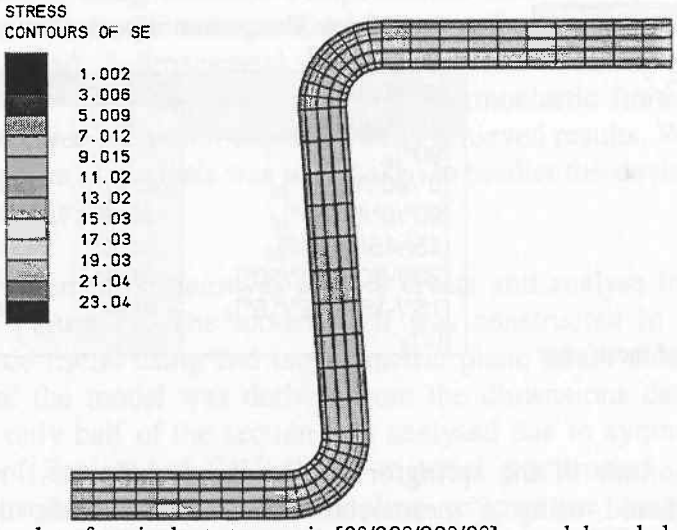

Figure 25. Contour plot of equivalent stresses in $[0°/90°/90°/0°]_{2S}$ model cooled from 120 to 20°C.

CONCLUSIONS

Two aspects of the roll forming process have been investigated using an experimental approach. The deformation length and its importance to the design and success of the process has been explained in the context of continuous fibre reinforced thermoplastic sheets. The kinematics of the roll forming process has been addressed using a finite strain approach. The theory pertaining to the computational analysis of the deformation length has been derived and will be formally outlined in future articles by the authors.

The experimental analysis of the deformation length has been performed by digitising the surfaces of a series of partially deformed sheets. The characteristic shape adopted by the sheets has been divided into three regions: region A, where the strip remains unaffected by the rolls or deformation downstream, region B, where the sheet experiences deformation but is not in contact with the forming rolls, and region C, where the sheet deforms while in contact with the rolls. The shape adopted by the sheets was found to differ from that encountered with sheet metals. At forming temperatures of 140°C or higher, the flange does not begin to develop until the sheet comes in contact with the rolls. From then on the sheet conforms to the geometry of the forming rolls by deforming in a trellis-like action. As the temperature is reduced the transverse bending required to form the flange takes place through a greater length as the materials response becomes more like an elastic solid.

Increasing the roll angle was found to have several important consequences. As the roll angle was increased from 20°→30°→40°, both the primary and secondary deformation lengths were found to increase. More importantly, as the roll angle was increased, the strain magnitudes in the flange increased resulting in thickness increases of up to 13.2% for the 40° roll setting. Each roll increment would obviously need to be considered when designing roll gap settings.

Rolled part conformance of various top-hat sections was found to be relatively poor. Both springback and springforward were observed in the sections formed through the entire process. A thermoelastic model was used to describe the distortion observed in the samples with only moderate success. The laminate configuration was found to have a significant effect on the magnitude of springforward and springback. While the magnitude of the distortion could not be accurately predicted by the model, the basic theory could be used to explain the experimentally achieved results. The model correctly predicts that as the fibres are aligned more acutely to the rolling axis, the distortion is minimised.

ACKNOWLEDGEMENTS

The authors gratefully acknowledge the support of the New Zealand Foundation for Research, Science and Technology. We also acknowledge the free supply of material from Mitsui-Toatsu (Japan).

REFERENCES

1. Cattanach, J.B. and Cogswell, F.N., Processing with aromatic polymer composites, *Developments in Reinforced Plastics*, Vol. 5. ed. G. Pritchard, Elsevier Applied Science Publishers, (1986), pp. 1-38.

2. Mander, S.J., Panton, S.M., Dykes, R.J., Bhattacharyya, D., Roll forming of sheet materials. In Composite Sheet Forming, ed. D. Bhattacharyya, Chapter 9. Composite Materials Series, Elsevier, Amsterdam, 1997.

3. Hobbs, R.M., Duncan, J.L., Roll forming, Metals Engineering Institute, American Society of metals, Ohio, USA (1979).

4. O'Leary, M., Space industrialisation, CRC press, Boca Raton, FL, USA (1982) pp. 102-105.

5. Ni, C.M., Gatny, D.A., Rahman, A., Application of finite element analysis to the curving or sweeping of roll formed sections for vehicle body structures, SAE Technical Paper Series, International Congress and Exposition, Detroit, Michigan, (1991).

6. Zhu, S.D., Theoretical and experimental analysis of roll forming, PhD Thesis, University of Auckland, February (1993).

7. Bhattacharyya, D., Smith, P.D., Yee, C.H., Collins, I.F., The prediction of deformation length in cold roll forming, Journal of Mechanical Working Technology, Vol. 9, March, (1984), pp. 181-191.

8. Nefussi, G., Gilormini, P., A simplified method for the simulation of cold roll forming, Int. J. Mech. Sci., 35, (1993) pp 867-874.

9. Zhu, S.D., Panton, S.M., Duncan, J.L., The effects of geometric variables in roll forming channel section, Proc. Inst. Of Mech Eng., Part B: Journal of Engineering Manufacture, Vol 210, (1996), pp. 127-134.

10. Martin, T.M., Christie, G.R., Bhattacharyya, D., Grid strain analysis. In Composite Sheet Forming, ed. D. Bhattacharyya, Chapter 9. Composite Materials Series, Elsevier, Amsterdam, (1997)

11. McGuinness, G.B., O'Bradaigh, C.M., Characterisation of the processing behaviour of unidirectional continuous fibre reinforced thermoplastic sheets, Presented at the 4th International Conference on Flow Processes in Composite Materials (FPCM96), University of Wales, Aberystwyth (1996)

12. Cattanach, J.B., Cuff, G., Cogswell, F.N., The processing of thermoplastics containing high loadings of land and continuous reinforcing fibres, Journal of Polymer Engineering, 6, (1986) pp. 345-361.

13. Rivlin, R.S., Networks of inextensible coords, in Non-linear Problems of Engineering, Academic Press, N.Y. (1964) pp. 51-64.

14. Green, A.E., Adkins, J.E., Large elastic deformations and non-linear continuum mechanics, Clarendon Press, Oxford (1960).

15. O'Neill, J.M., Rogers, T.G., Spencer, A.J.M, Thermally induced distortions in the moulding of laminated channels sections. Math. Eng. Ind., 2, (1988) pp. 65-72.

16. Spencer, A.J.M, Watson, P., Rogers, T.G., Thermoelastic distortions in laminated anisotropic tubes and channel sections, Journal of Thermal Stresses, 15, (1992) pp. 129-141.

17. Spencer, A.J.M, Watson, P., Rogers, T.G., Mathematical analysis of of the springback effect in laminated thermoplastic channel sections, Composites Manufacturing, 2, (1991) pp. 253-258.

18. Zahlan, N., O'Neill, J.M., Design and fabrication of composite components; the spring-forward phenomenon, *Composites* 20, Num. 1, January 1989.

19. Cuff, G., 'Fibre-reinforced industrial thermoplastic composites', Woodhead Publishers Ltd., Cambridge, UK, 1995.